PHILOSOPHICAL TRANSACTIONS OF THE ROYAL SOCIETY A MATHEMATICAL, PHYSICAL & ENGINEERING SCIENCES

The Dependence of the Shape and Stability of Captive Rotating Drops on Multiple Parameters

L. H. Ungar and R. A. Brown

Phil. Trans. R. Soc. Lond. A 1982 **306**, 347-370
doi: 10.1098/rsta.1982.0090

Phil. Trans. R. Soc. Lond. A **306**, 347–370 (1982) [347]
Printed in Great Britain

THE DEPENDENCE OF THE SHAPE AND STABILITY OF CAPTIVE ROTATING DROPS ON MULTIPLE PARAMETERS

BY L. H. UNGAR AND R. A. BROWN
Department of Chemical Engineering, Massachusetts Institute of Technology, Cambridge, Massachusetts 02139, *U.S.A.*

(*Communicated by K. Stewartson, F.R.S. – Received* 28 *September* 1981)

CONTENTS

The dependence of the shape and stability of rigidly rotating captive drops on multiple parameters is analysed by applying asymptotic and computer-aided techniques from bifurcation theory to the Young–Laplace equation which governs meniscus shape. In accordance with Brown and Scriven, equilibrium shapes for drops with the volume of a cylinder and without gravity are grouped into families of like symmetry that branch from the cylindrical shape at specific values of rotation rate, measured by the rotational Bond number Σ. Here, the evolution of these families with changes in drop volume $\mathscr{V}$, drop length B, and gravitational Bond number G is presented. Criteria are laid out for

predicting drop stability from the evolution of shape families in this parameter-space and they circumvent much of the extensive solution of eigenproblems used previously.

Asymptotic analysis describes drops slightly different from the cylindrical ones and shows that some shape bifurcations from cylinders to wavy, axisymmetric menisci are ruptured by small changes in drop volume or gravity. Near these points at least one of the shape families singularly develops a fold or limit point.

Numerical methods couple finite-element representation of drop shape which is valid for a wide range of parameters with computer-implemented techniques for tracking shape families. An algorithm is presented that calculates, in two parameters, the loci of bifurcation or limit points; this is used to map drop stability for the four-dimensional parameter space $(\Sigma, \mathscr{V}, B, G)$. The numerical and asymptotic results compare well in the small region of parameters where the latter are valid. An exchange of axisymmetric mode for instability is predicted numerically for drop volumes much smaller than that of a cylinder.

1. Introduction

The calculation of the shape and stability of interfaces that separate immiscible and static fluids presents problems that have long fascinated researchers. Problems in capillary statics have simple mathematical statements and the results have wide application. The shapes of such menisci are governed by the nonlinear Young–Laplace equation or, alternatively, are given as extrema of the potential energy function that describes the body forces shaping the interface. The solution of the Young–Laplace equation is difficult and, usually, requires computer-aided calculation. The organization of equilibrium menisci can also be complex; multiple or no equilibrium shapes have been found in an increasing number of capillary problems. The occurrences of shape multiplicity or loss of equilibrium are intimately connected with the stability of the interface.

Interfacial stability is controlled by the response of the potential energy to changes in the shape of the meniscus and, for small-amplitude shape disturbances, is governed mathematically by a linear eigenproblem. Traditional studies of interfacial stability (Gillete & Dyson 1971; Pitts 1973, 1976) are founded on analysis of this eigenproblem. Others use the equivalence between the mathematical questions of neutral stability with respect to a certain shape perturbation and of bifurcation to a new shape family that, at lowest-order, resembles the same perturbation superimposed on the original shape.

Ideas and analyses from the field of bifurcation theory have been applied with success to interfacial problems controlled by a single parameter (Pimbley 1976; Majumdar & Michael 1976; Brown & Scriven 1980*a–c*; Benner *et al.* 1980). In several problems, menisci have been grouped into families based on interfacial symmetry, and the connectivity and evolution of these families have been studied as the parameter, say Σ, was varied. The joining of two shape families and the loss of one were explained by the occurrence of bifurcation points and limit points, respectively, as Σ changed. These two possibilities are common in bifurcation analysis (Thompson & Hunt 1973) and are sketched in figure 1 with ϵ representing a measure of interface shape.

Varying a second parameter in a meniscus problem may alter dramatically the connectivity of the equilibrium families and change the stability characteristics of the meniscus. Variations of second parameters rupture certain bifurcation points, causing imperfect or perturbed bifurcation (Keener & Keller 1973; Thompson & Hunt 1973; Reiss 1977). In this paper we extend the asymptotic and numerical techniques developed in Brown & Scriven (1980*a*; hereafter referred to as I) to analyse the dependence of meniscus shape on multiple parameters. The asymptotic methods are based on the perturbation procedures described in Matkowsky & Reiss (1977) and Iooss & Joseph (1980) and are designed to account for the splitting of a bifurcation

point as a second parameter is varied. Our numerical methods, like those in I, combine finite-element representation of drop shape with computer-implemented techniques for tracking shape families. Here, more efficient methods are used for tracking families through bifurcation and limit points. Another algorithm calculates directly sets of singular points – either bifurcation or limit points – in two parameters and makes possible calculation of the limits of shape stability in many parameters. Although the techniques of bifurcation analysis used here apply to non-conservative systems, the conservative framework of static meniscus problems allows, in many cases, for the stability of the menisci to be inferred directly from the connectivity of the shape families, obviating many of the eigenvalue calculations performed in I.

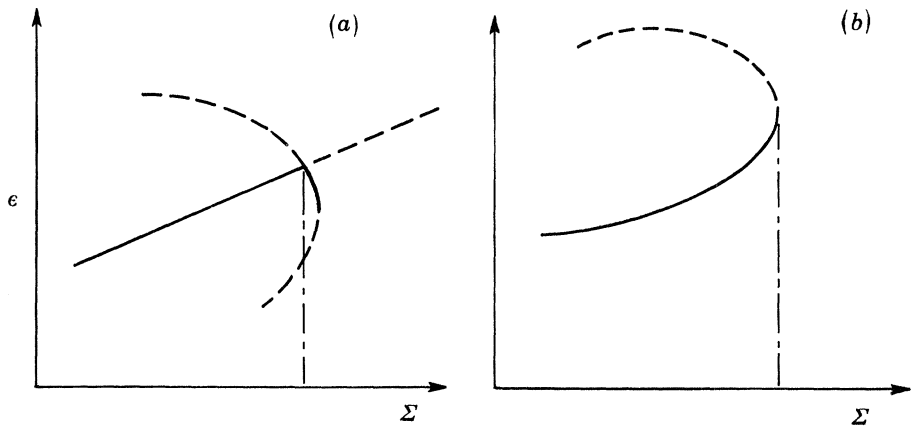

FIGURE 1. Shape family representations of (*a*) bifurcation and (*b*) limit points. Here Σ is a parameter and ϵ is a measure of the distortion of the meniscus. Stable shapes are shown by a solid curve; unstable shapes by a dashed curve.

The multiple equilibrium menisci of several capillary problems have been characterized by the volume of fluid enclosed by the interface. Translationally symmetric pendent drops (Majumdar & Michael 1976) and neutrally buoyant liquid fillets (Brown & Scriven 1980*c*) of fixed volume both lose stability at the liquid volume where a family of three-dimensional sinuous shapes joins the two-dimensional forms. Most axisymmetric pendent drops (Michael & Williams 1976; Michael 1981) and liquid drops hanging from inclined tubes (Lawal & Brown 1982*a*) lose stability at limit points in terms of drop volume.

The shape and stability of rigidly rotating free drops depend entirely on a single parameter, the rotational Bond number Σ, that measures the strength of the centrifugal pressure field relative to surface tension. Brown & Scriven (1980*b*) mapped out the equilibrium forms of such a drop by computer-aided techniques like those in I. Shape and stability were determined by solving the eigenvalue problem for each equilibrium form.

The equilibrium shapes and stability of a drop held captive between co-rotating solid faces are governed by four parameters: the distance between the solid faces, the dimensionless drop volume ($\mathscr{V}$), the rotational Bond number Σ, and the gravitational Bond number G, which measures the relative importance of gravity and surface tension in setting drop shape. In I, the shapes and stability of captive drops were calculated for ranges of Σ and $\mathscr{V}$, but without gravity. In this limit, a cylindrical drop (a special value of $\mathscr{V}$) that attaches to the solid form is an equilibrium shape for all rotational Bond numbers. New families of either axisymmetric or non-axisymmetric drop shapes branch from the cylindrical ones at specific values of Σ. Numerical

calculations in I show that changing the volume of the drop breaks the cylindrical drop family; equilibrium drop shapes were not calculated for rotation rates above a maximum value of Σ, where a limit point appeared in the shape family.

We focus our analysis on the captive rotating drop; the appropriate form of the Young–Laplace equation is given in § 2. Asymptotic analysis outlined in § 3 shows the rupturing of the family of cylindrical drops at bifurcation points to axisymmetric shape families as the drop volume $\mathscr{V}$ is changed. The addition of gravity also splits the cylindrical drop family but at the branch points to *different* families of axisymmetric shapes. We relate this result to calculations of Coriell *et al.* (1977) for non-rotating liquid zones influenced by gravity.

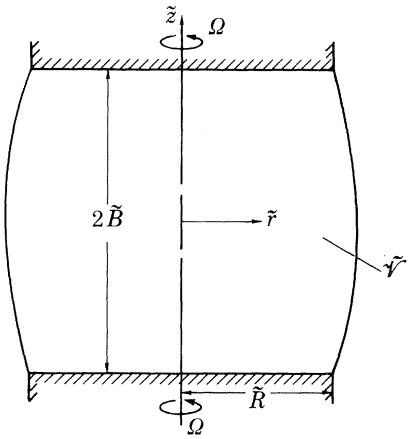

FIGURE 2. A rotating captive drop of volume $\tilde{\mathscr{V}}$ with its dimensions.

The numerical algorithms for tracking shape families and singular points are given in § 4, and the arguments for obtaining shape stability from plots of family connectivity are discussed in § 5. The asymptotic and numerical calculations for nearly cylindrical drops are compared in § 6, and the ranges of validity of the perturbation results are established. Numerical calculations are presented for the evolution of axisymmetric shape families over ranges of the four parameters and, in several limits, are compared with previous stability analyses.

2. EQUILIBRIUM DROP SHAPES

We consider a drop of volume $\tilde{\mathscr{V}}$ in a gap of length $2\tilde{B}$ between two coaxial solid faces of radius $\tilde{R}$, both of which are rotating at angular velocity Ω. The liquid wets the two faces, and the meniscus is assumed to pin at circular contact lines of radius $\tilde{R}$. The surrounding fluid exerts only a uniform pressure on the captive drop.

The shape of the drop is represented in cylindrical coordinates as $\tilde{r} = \tilde{f}(z, \theta)$; see figure 2. The Young–Laplace equation for meniscus shape is derived in I, the effects of gravity being neglected. This derivation is easily repeated with the inclusion of a potential that increases with $\tilde{z}$ and yields the dimensionless equation

$$4\Sigma f^2 + 2K + Gz = \frac{2f_\theta f_z f_{\theta z} + f(1 + f_z^2 + f_\theta^2/f^2) - (f^2 + f_\theta^2) f_{zz} - (1 + f_z^2) f_{\theta\theta}}{f^2[1 + f_z^2 + f_\theta^2/f^2]^{\frac{3}{2}}}, \tag{2.1}$$

where $f \equiv \tilde{f}(z, \theta)/\tilde{R}$ and $z \equiv \tilde{z}/R$ are dimensionless variables, $\Sigma \equiv \tilde{R}^3\Omega^2\Delta\rho/8\sigma$ is the rotational Bond number, $K \equiv \tilde{R}\Delta p_0/2\sigma$ is the dimensionless reference pressure, and $G \equiv \tilde{R}^2 g\Delta\rho/\sigma$ is the

gravitational Bond number. The subscripts z and θ denote partial differentiation, i.e. $f_\theta \equiv \partial f/\partial\theta$. In these definitions σ is the surface tension, $\Delta\rho$ is the density difference between the drop and the surroundings, g is the acceleration due to gravity, and Δp_0 is the datum pressure difference, being that which would occur if the meniscus reached the axis of rotation.

The wetting conditions at the edges of the circular faces are, in dimensionless form,

$$f(-B,\theta) = f(B,\theta) = 1, \quad 0 \leqslant \theta \leqslant \pi, \tag{2.2}$$

where $B \equiv \tilde{B}/\tilde{R}$. As in I, we assume the drop shape has a plane of reflective symmetry that passes through the axis of rotation and through $\theta = 0$; then

$$f_\theta(z,0) = f_\theta(z,\pi) = 0, \quad -B \leqslant z \leqslant B. \tag{2.3}$$

The reference pressure difference K is determined from the constraint that the meniscus encloses a fixed dimensionless volume $\mathscr{V} \equiv \tilde{\mathscr{V}}/\tilde{R}^3$ for half of the drop:

$$\mathscr{V} = \frac{1}{2}\int_0^\pi \int_{-B}^{B} f^2 \,\mathrm{d}z\,\mathrm{d}\theta. \tag{2.4}$$

3. Perturbations about a cylindrical drop

In the absence of gravity a perfectly cylindrical drop is an equilibrium form for all rotation rates. The corresponding solution to (2.1)–(2.4) is

$$f(\theta,z) = 1, \quad K = \tfrac{1}{2} - 2\Sigma, \tag{3.1}$$

for $G = 0$, $\mathscr{V} = \pi B$, and all values of Σ. Brown & Scriven (I) have exploited this result to study the shape and stability of these cylinders as Σ changes, but with $\mathscr{V}$ and G held fixed.

The asymptotic analysis in I and the studies of variation of $\mathscr{V}$ and G presented in this paper are both embedded in two-variable expansions of the unknowns $(f(z,\theta), K)$ and parameters $(\Sigma, G, \mathscr{V})$ in terms of an amplitude parameter ϵ and a scaling parameter δ:

$$\begin{bmatrix} f(z,\theta;\epsilon,\delta) \\ K(\epsilon,\delta) \\ \Sigma(\epsilon,\delta) \\ G(\epsilon,\delta) \\ \mathscr{V}(\epsilon,\delta) \end{bmatrix} = \sum_{n=0}^{\infty}\sum_{m=0}^{\infty} \frac{\epsilon^n \delta^m}{n!\,m!} \begin{bmatrix} f_m^{(n)} \\ K_m^{(n)} \\ \Sigma_m^{(n)} \\ G_m^{(n)} \\ \mathscr{V}_m^{(n)} \end{bmatrix}. \tag{3.2}$$

In these expansions, ϵ measures the amplitude of the difference between the known shapes in a family of cylindrical drops and those in a bifurcating family; the parameter δ scales the variation of a particular shape family with the changing of either G or $\mathscr{V}$ and will be identified as one of these parameters to a power. For brevity, the solution of the (n,m)th-order problem is denoted as $\boldsymbol{v}_m^{(n)} \equiv (f_m^{(n)}(z,\theta), K_m^{(n)})$.

The first term in each expansion always corresponds to the cylindrical shape ($f_0^{(0)} = 1$, $K_0^{(0)} = \frac{1}{2} - \Sigma_0^{(0)}$, $G_0^{(0)} = 0$, $\mathscr{V}_0^{(0)} = \pi B$) and is valid for all values of $\Sigma_0^{(0)}$ and B. Substituting (3.2) into equations (2.1)–(2.4) yields non-homogeneous linear partial differential equations of the form

$$\mathscr{L}\boldsymbol{v}_j^{(i)} \equiv \begin{bmatrix} (\nabla^2 + \gamma^2)(\ ) & 2 \\ \displaystyle\int_0^\pi \int_{-B}^{B} (\ )\,\mathrm{d}z\,\mathrm{d}\theta & 0 \end{bmatrix} \begin{bmatrix} f_j^{(i)} \\ K_j^{(i)} \end{bmatrix} = \boldsymbol{d}_j^{(i)}(G_j^{(i)}, \mathscr{V}_j^{(i)}) \tag{3.3}$$

where $\gamma^2 \equiv 1 + 8\Sigma_0^{(0)}$, $\nabla^2 \equiv \partial^2/\partial z^2 + \partial^2/\partial\theta^2$, and $\boldsymbol{d}_j^{(i)}$ is the vector calculated at each order from the non-homogeneous terms in (2.1) and lower-order terms in the expansion (3.2).

For analysis of bifurcation points the three vectors $\boldsymbol{d}_0^{(1)}$, $\boldsymbol{d}_0^{(2)}$, $\boldsymbol{d}_0^{(3)}$ are needed:

$$\left.\begin{aligned}
\boldsymbol{d}_0^{(1)}(G_0^{(1)}, \mathscr{V}_0^{(1)}) &\equiv \begin{bmatrix} -G_0^{(1)} z \\ V_0^{(1)} \end{bmatrix}, \\
\boldsymbol{d}_0^{(2)}(G_0^{(2)}, \mathscr{V}_0^{(2)}) &\equiv \begin{bmatrix} (3-\gamma^2) f_0^{(1)2} - f_{0z}^{(1)2} + f_{0\theta}^{(1)2} - 16\Sigma_0^{(1)} f_0^{(1)} + 4 f_0^{(1)} f_{0\theta\theta}^{(1)} - G_0^{(2)} z \\ -\frac{1}{2}\int_0^{\pi}\int_{-B}^{+B} f_0^{(1)2}\,\mathrm{d}z\,\mathrm{d}\theta + V_0^{(2)} \end{bmatrix}, \\
\boldsymbol{d}_0^{(3)}(G_0^{(3)}, \mathscr{V}_0^{(3)}) &\equiv \begin{bmatrix} -24(\Sigma_0^{(1)} f_0^{(2)} + \Sigma_0^{(2)} f_0^{(1)} + \Sigma_0^{(1)} f_0^{(1)2}) + 3(3-\gamma^2) f_0^{(1)} f_0^{(2)} \\ -3 f_{0z}^{(1)} f_{0z}^{(2)} + 3 f_0^{(1)} f_{0z}^{(1)2} + 9 f_{0z}^{(1)2} f_{0zz}^{(1)} \\ +3(f_{0\theta}^{(1)} f_{0\theta}^{(2)} + f_{0z}^{(1)2} f_{0\theta\theta}^{(1)} + f_{0\theta}^{(1)2} f_{0zz}^{(1)} - 6 f_0^{(1)2} f_{0\theta\theta}^{(1)}) \\ +6(f_0^{(1)} f_{0\theta\theta}^{(2)} + f_0^{(2)} f_{0\theta\theta}^{(1)} + 2 f_{0\theta}^{(1)} f_{0z}^{(1)} f_{0\theta z}^{(1)} - f_0^{(1)3}) \\ +9 f_{0\theta}^{(1)2} f_{0\theta\theta}^{(1)} - 9 f_0^{(1)} f_{0\theta}^{(1)2} - G_0^{(3)} z \\ V_0^{(3)} \end{bmatrix}.
\end{aligned}\right\} \tag{3.4}$$

The boundary conditions (2.2), (2.3) reduce at each order to

$$\left.\begin{aligned} f_j^{(i)}(-B,\theta) &= f_j^{(i)}(B,\theta) = 0, \quad 0 \leqslant \theta \leqslant \pi, \\ f_{j\theta}^{(i)}(z,0) &= f_{j\theta}^{(i)}(z,\pi) = 0, \quad -B \leqslant z \leqslant B. \end{aligned}\right\} \tag{3.5}$$

The homogeneous version of equations (3.3)–(3.5) is symmetric in the inner product defined as

$$\langle \boldsymbol{\beta}_1, \boldsymbol{\beta}_2 \rangle \equiv \int_0^{\pi}\int_{-B}^{+B} g_1(z,\theta)\, g_2(z,\theta)\,\mathrm{d}z\,\mathrm{d}\theta + 2k_1 k_2, \tag{3.6}$$

where $\boldsymbol{\beta}_1^{\mathrm{T}} \equiv (g_1(z,\theta), k_1)$ and $\boldsymbol{\beta}_2^{\mathrm{T}} \equiv (g_2(z,\theta), k_2)$. At values of B and $\Sigma_0^{(0)}$ where the homogeneous problem has a non-trivial solution $\boldsymbol{\zeta}^{\mathrm{T}} \equiv (\phi(z,\theta), c)$, known as a null vector, the non-homogeneous equation set (3.3)–(3.5) at (i,j)th order has a bounded solution only when the solvability criterion

$$\langle \boldsymbol{\zeta}, \boldsymbol{d}_j^{(i)} \rangle = 0 \tag{3.7}$$

TABLE 1. ASYMPTOTIC RESULTS FOR BIFURCATION FOR THE FAMILY OF CYLINDRICAL ROTATING DROPS; $G = 0$ AND $\mathscr{V} = \pi B$

shape families	bifurcation points		eigenfunctions	
ymmetric (ax.)				
i) reflectively symmetric (r.s.)	$\Sigma_{0ns}^{(0)} = \frac{1}{8}\alpha_{ns}^2/B^2 - \frac{1}{8}$, $\alpha_{ns}\cot\alpha_{ns} = 1$, $n = 1, 2, \ldots$	(3.8)	$\boldsymbol{v}_{0ns}^{(1)} = \begin{bmatrix} f_{0ns}^{(1)}(z) \\ K_{0ns}^{(1)} \end{bmatrix}$ $= (\pi B \sin^2\alpha_s)^{-\frac{1}{2}} \begin{bmatrix} \cos(\alpha_{ns} z/B) - \cos(\alpha_{ns}) \\ \alpha_{ns}\sin(\alpha_{ns})/2B^2 \end{bmatrix}$	(3.9)
ii) reflectively antisymmetric (r.a.)	$\Sigma_{0na}^{(0)} = \frac{1}{8}n^2\pi^2/B^2 - \frac{1}{8}$, $n = 1, 2, \ldots$	(3.10)	$\boldsymbol{v}_{0na}^{(1)} = \begin{bmatrix} f_{0na}^{(1)}(z) \\ K_{0na}^{(1)} \end{bmatrix} = (\pi B)^{-\frac{1}{2}} \begin{bmatrix} \sin(n\pi z/B) \\ 0 \end{bmatrix}$	(3.11)
axisymmetric (n.ax.)				
i) reflectively symmetric (r.s.)	$\Sigma_{0nks}^{(0)} = \frac{1}{32}n^2\pi^2/B^2 + \frac{1}{8}k^2 - \frac{1}{8}$, $n = 2, 4, 6, \ldots$, $k = 1, 2, \ldots$	(3.12)	$\boldsymbol{v}_{0nks}^{(1)} = \begin{bmatrix} f_{0nks}^{(1)}(z,\theta) \\ K_{0nks}^{(1)} \end{bmatrix}$ $= \left(\frac{2}{\pi B}\right)^{\frac{1}{2}} \begin{bmatrix} \sin(n\pi z/2B)\cos(k\theta) \\ 0 \end{bmatrix}$	(3.13)
ii) reflectively antisymmetric (r.a.)	$\Sigma_{0nka}^{(0)} = \frac{1}{32}n^2\pi^2/B^2 + \frac{1}{8}k^2 - \frac{1}{8}$, $n = 1, 3, 5, \ldots$, $k = 1, 2, \ldots$	(3.14)	$\boldsymbol{v}_{0nka}^{(1)} = \begin{bmatrix} f_{0nka}^{(1)}(z,\theta) \\ K_{0nka}^{(1)} \end{bmatrix}$ $= \left(\frac{2}{\pi B}\right)^{\frac{1}{2}} \begin{bmatrix} \cos(n\pi z/2B)\cos(k\theta) \\ 0 \end{bmatrix}$	(3.15)

is satisfied (Friedman 1956). These conditions are central to both the asymptotic analysis of bifurcation and to the numerical schemes for tracking singular points.

When the expansions in the scaling parameter δ are neglected, and G and $\mathscr{V}$ are fixed at their values for the cylindrical shape family, our analysis of equations (3.3)–(3.5) reduces to the work presented in I, and the solvability conditions (3.7) determine how the bifurcating shape families evolve in Σ near the bifurcation point; i.e. they are used to determine the constants $\{\Sigma_0^{(i)}\}$. We refer to this case as unperturbed bifurcation. To calculate the changes in the cylindrical shapes brought on by varying G (or $\mathscr{V}$) the expansions in the amplitude parameter ϵ are neglected and the solvability conditions are used to determine the relation between the variation in G (or $\mathscr{V}$) and the scaling parameter δ. Matkowsky & Reiss (1977) called the case when δ and G (or $\mathscr{V}$) are related nonlinearly a singular perturbation of the unperturbed bifurcation.

Corrected results of the analysis of the unperturbed bifurcation from I are summarized in § 3.1. The calculations of the effects of varying G and $\mathscr{V}$ follow in § 3.2 and 3.3.

3.1. *Unperturbed bifurcation: the cylindrical drop*

When the expansions for G and $\mathscr{V}$ are neglected the vector $\boldsymbol{d}_0^{(1)}(0,0)$ is zero and equations (3.3)–(3.5) reduce to a linear eigenproblem for eigenvalues $\{\Sigma_{0n}^{(0)}\}$ and eigenvectors $\boldsymbol{v}_{0n}^{(1)\mathrm{T}} \equiv (f_{0n}^{(1)}(z,\theta), K_{0n}^{(1)})$. The values of $\{\Sigma_{0n}^{(0)}\}$ give the locations of bifurcation points between the family of cylindrical drops and new families of shapes with less symmetry. These points were classified in I according to the symmetry of $f_{0n}^{(1)}(z,\theta)$ and are summarized in table 1 by equations (3.8)–(3.15). The eigenvectors have been normalized by using the amplitude defined as

$$\epsilon \equiv \langle \boldsymbol{v} - \boldsymbol{v}_{0n}^{(1)}, \boldsymbol{v}_{0n}^{(1)} \rangle. \tag{3.16}$$

Axisymmetric drops occur in two sets of families which differ in shape symmetry with respect to reflexions about the plane perpendicular to the axis of rotation at $z = 0$. One set has shapes that are reflectively symmetric (r.s.); the other has shapes that are reflectively anti-symmetric (r.a.). The other two sets of shape families are made up of non-axisymmetric (n.ax.) equilibrium forms again differing by their symmetry with respect to the midplane of the drop. As shown below, the symmetry of the equilibrium shapes in a family dictates how the family evolves with changes in parameters: different shape families show qualitatively different behaviour when either G or $\mathscr{V}$ is changed.

The evolution of the various shape families in the ϵ, Σ-plane is determined by calculating the constants $(\Sigma_0^{(1)}, \Sigma_0^{(2)}, \ldots)$. For the axisymmetric shape families the first terms are

$$\text{type ax.–r.s.: } \Sigma_{0ns}^{(1)} = \frac{-1}{48\gamma B(\pi B)^{\frac{1}{2}}}\left[\frac{4(3-\gamma^2)}{\sin^2(\gamma B)} + 3 + \gamma^2\right], \tag{3.17}$$

$$\text{type ax.–r.a.: } \Sigma_{0na}^{(1)} = 0, \tag{3.18}$$

where equation (3.17) is the corrected result of equation (4.12) in I. Projected in the ϵ, Σ-plane the ax.–r.s. family cuts the cylindrical family at an angle that depends on the dimensionless length of the drop. At $2B \approx 4.07$ the projections of the two families are exactly perpendicular and, at higher values of B, the angle changes sign. This evolution with B of the ax.–r.s. family at the bifurcation point is explained by a limit point in the r.s. family near the bifurcation point. As B is increased the limit point shifts closer to the branch point and at $2B \approx 4.07$ is coincident with it. At higher values of B the limit point is on the opposite side of the bifurcation point. This sequence is demonstrated by numerical calculations shown in figure 5.

The direction of bifurcation in the ϵ, Σ-plane for the ax.–r.a. families is dictated by the quadratic coefficient $\Sigma^{(2)}_{0na}$,

$$\Sigma^{(2)}_{0na} = -(1/32\pi B)\,[18 + 8\gamma^2 + 3\gamma^4], \tag{3.19}$$

which is always negative. Analysis of the bifurcating families of non-axisymmetric shapes has not been carried out to second order in ϵ; however, numerical results presented in I indicate that the first two shape-families bifurcate subcritically ($\Sigma^{(1)}_0 = 0$, $\Sigma^{(2)}_0 < 0$) when the drop has the volume of a cylinder.

3.2. *Perturbed bifurcation: changes in volume and gravity*

The variation of the cylindrical shapes with changes in G or $\mathscr{V}$ is calculated by expanding $f(z, \theta)$ and K in terms of one of these parameters about (3.1). Formally, this is accomplished by identifying δ in (3.2) with either $\Delta\mathscr{V} \equiv (\mathscr{V} - \pi B)$ or G and by neglecting the expansion for $G(\Delta\mathscr{V})$ and Σ. The variations in drop shape and reference pressure due to a small value of G are

$$\boldsymbol{v}^{(0)}_1 \equiv \frac{-1}{\gamma^2 \sin(\gamma B)} \begin{bmatrix} B\sin(\gamma z) - z\sin(\gamma B) \\ 0 \end{bmatrix}, \tag{3.20}$$

with $\gamma^2 \equiv 1 + 8\Sigma$. A small change in $\mathscr{V}$ gives the correction

$$\boldsymbol{v}^{(0)}_1 \equiv \frac{-1}{2\pi B[\cos(\gamma B) - \sin(\gamma B)/\gamma B]} \begin{bmatrix} \cos(\gamma z) - \cos(\gamma B) \\ \frac{1}{2}\gamma^2 \cos(\gamma B) \end{bmatrix}. \tag{3.21}$$

The shape corrections (3.20), (3.21) for changes in G and $\mathscr{V}$ become infinite near the r.a. and r.s. bifurcation points, respectively. Near these points the regular expansion that results from scaling δ proportional to either G or $\Delta\mathscr{V}$ is unreasonable. The singular behaviour of the shape families at these points is qualitatively clear by analogy with other work (Keener & Keller 1973; Reiss 1977); as G or $\mathscr{V}$ is varied, the bifurcation point splits into separate curves and a limit point is created.

To develop expansions valid near the axisymmetric bifurcation points we start from (3.2) with $n = 0$ and use the solvability criteria (3.7) to calculate what terms in the expansions for G or $\mathscr{V}$ in terms of δ must be zero so that the solutions are bounded. This approach yields the same result as the inner expansion in the singular perturbation technique of Matkowsky & Reiss (1977), as well as the appropriate scaling between the parameter (G or $\mathscr{V}$) and δ. In the next two subsections the results are presented for changes in $\mathscr{V}$ near the ax.–r.s. bifurcation point and in G near the ax.–r.a. bifurcation point. There is no need for rescaling the parameters near the non-axisymmetric bifurcation points (3.12), (3.14) since the corrections to the drop shapes (3.20), (3.21) are bounded there. The variation of these points with changes in G and $\mathscr{V}$, the variations of ax.–r.a. points in $\mathscr{V}$, and of ax.–r.s. points in G, are presented last.

(*a*) *Perturbations in $\mathscr{V}$ near ax.–r.s. bifurcation points*

When the expansion for G is neglected in (3.2), the first-order problem becomes (3.3) with $\boldsymbol{d}^{(0)}_1 \equiv (0, \mathscr{V}^{(0)}_1)$. The homogeneous problem is the same as solved in the analysis of unperturbed bifurcation and is singular at the ax.–r.s. bifurcation points. The non-homogeneous problem has a bounded solution at $\Sigma = \Sigma^{(0)}_{0ns}$ if

$$\langle \boldsymbol{v}^{(1)}_{0ns}, \boldsymbol{d}^{(0)}_1 (0, \mathscr{V}^{(0)}_1) \rangle = 0, \tag{3.22}$$

where $\boldsymbol{v}^{(1)}_{0ns}$ is the solution of the unperturbed problem (see table 1). Equation (3.22) has a solution only when $\mathscr{V}^{(0)}_1 = 0$. Thus the first-order problem becomes homogeneous ($\boldsymbol{d}^{(0)}_1 = 0$) and its

solution is $\boldsymbol{v}_1^{(0)} = A\boldsymbol{v}_{0ns}^{(1)} \equiv A(\phi, c)^{\mathrm{T}}$ where A is an unknown amplitude. Proceeding to the second-order problem gives the solvability criteria

$$\langle \boldsymbol{v}_{0ns}^{(1)}, \boldsymbol{d}_2^{(0)}(0, \mathscr{V}_2^{(0)}) \rangle = [(3-\gamma^2)\,\mathscr{I}(\phi^3) - \mathscr{I}(\phi_z^2\phi) - 2c]\,A^2 - 16\Sigma_1^{(0)}A + 2\mathscr{V}_2^{(0)}c = 0, \quad (3.23)$$

with $\mathscr{I}(\phi) \equiv \int_0^{\pi}\int_{-B}^{B}(\,)\,\mathrm{d}z\,\mathrm{d}\theta$. This equation is quadratic in A in terms of $\Sigma_1^{(0)}$ for any value of $\mathscr{V}_2^{(0)}$. We set $\mathscr{V}_2^{(0)} = 1$ without loss of generality. Then specifying δ *sets* the value of $\mathscr{V}$ and setting $\Sigma_1^{(0)}$ gives a distance in Σ from the ax.–r.s. bifurcation point; see equation (3.2). For each pair δ and $\Sigma_1^{(0)}$, there may be either no, one or two values of A that satisfy (3.23).

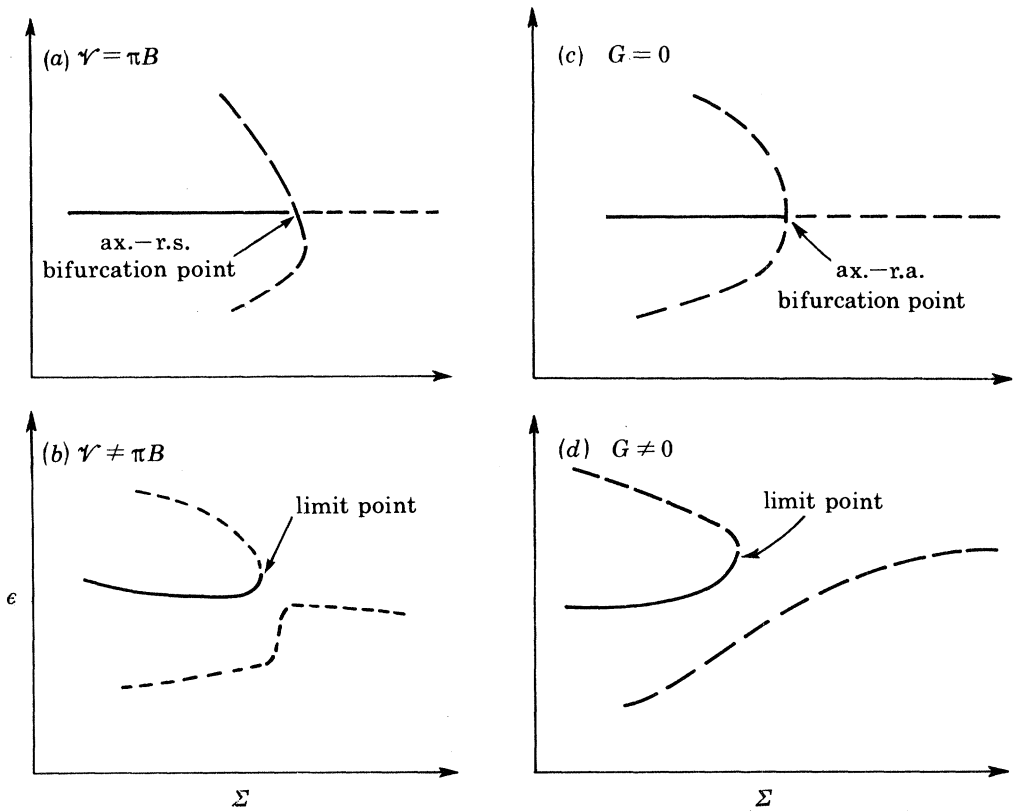

FIGURE 3. Rupturing of bifurcation points by changes in parameters: (*a*), (*b*) separation of ax.–r.s. bifurcation point with change in $\mathscr{V}$; (*c*), (*d*) separation of ax.–r.a. bifurcation point with change in G.

The regions of no solutions enclose the ax.–r.s. bifurcation points for any value of ϵ, with $\delta \equiv (2|\mathscr{V} - \pi B|)^{\frac{1}{2}}$. The ax.–r.s. points are each split locally into two distinct limit points for drops of any volume except πB. The loci of these limit points are given by solving the condition for a vanishing discriminant of (3.23) for $\Sigma_1^{(0)}$. This result is

$$\Sigma_1^{(0)} = \left[\frac{\gamma_{ns}\,\Sigma_{0ns}^{(1)}}{4(\pi B^3)^{\frac{1}{2}}}\right]^{\frac{1}{2}}, \quad (3.24)$$

where $\gamma_{ns}^2 \equiv 1 + 8\Sigma_{0ns}^{(0)}$, and $\Sigma_{0ns}^{(1)}$ is defined by equation (3.17). The splitting of this bifurcation point is sketched in figures 3*a*, *b*.

(*b*) *Perturbations in G near ax.–r.a. bifurcation points*

The analysis of the cylindrical-shape family near the ax.–r.a. bifurcation points follows that in the previous section, except the expansion for G in (3.2) is retained and the one for $\mathscr{V}$ is neglected. The conditions (3.7) for bounded solutions of first- and second-order problems at $\Sigma_0^{(0)} = \Sigma_{0na}^{(0)}$ require that

$$G_1^{(0)} = G_2^{(0)} = \Sigma_1^{(0)} = 0. \tag{3.25}$$

TABLE 2. COEFFICIENTS FOR THE RATE OF CHANGE OF UNBROKEN BIFURCATION POINTS WITH CHANGES IN DROP VOLUME $\mathscr{V}$ OR GRAVITATIONAL BOND NUMBER G

type ax.–r.s. bifurcation point: variation in G	$\Sigma_1^{(0)} = 0$
type ax.–r.a. bifurcation point: variation in $\mathscr{V}$	$\Sigma_1^{(0)} = \dfrac{3-\gamma^2}{16\pi B}$
type n.ax.–r.a. bifurcation point: variation in G	$\Sigma_1^{(0)} = 0$
type n.ax.–r.a. bifurcation point: variation in $\mathscr{V}$ ($n = 1$ only)	$\Sigma_1^{(0)} = \dfrac{(3-\gamma^2-2k^3)\left[\dfrac{\sin\alpha}{\alpha}+\left(\dfrac{\alpha^2}{\pi^2}-1\right)\cos\alpha\right]-\gamma^2\dfrac{\sin\alpha}{2\alpha}}{32\pi B\left(\cos\alpha-\dfrac{\sin\alpha}{\alpha}\right)\left(\dfrac{\alpha^2}{\pi^2}-1\right)}$, $\alpha \equiv \gamma B$

Solutions of the first- and second-order problems are $\boldsymbol{v}_1^{(0)} = A\boldsymbol{v}_0^{(1)} \equiv A(\phi_1, 0)^{\mathrm{T}}$ and $\boldsymbol{v}_2^{(0)} = A^2\boldsymbol{v}_0^{(2)} \equiv A^2(\phi_2, 0)^{\mathrm{T}}$, respectively, where A is again an amplitude. The solvability criteria for the third-order problem yields a cubic equation for A in terms of $\Sigma_2^{(0)}$ and $G_3^{(0)}$, which is solvable for any non-zero value of $G_3^{(0)}$. Setting $G_3^{(0)} = 1$ gives

$$\begin{aligned}\langle \boldsymbol{\zeta}, \boldsymbol{d}_3^{(0)}(G_3^{(0)}, 0)\rangle = [3(3-\gamma^2)\mathscr{I}(\phi_1^2\phi_2) - 6\mathscr{I}(\phi_1^4) - 3\mathscr{I}(\phi_{1z}\phi_{2z}\phi_1) - 6\mathscr{I}(\phi_1^2\phi_{1z}^2) \\ + 9\mathscr{I}(\phi_{1z}^2\phi_{1zz}\phi_1)]A^3 - 24\Sigma_1^{(0)}\mathscr{I}(\phi^2)A - G_3^{(0)}\mathscr{I}(z\phi_1) = 0.\end{aligned} \tag{3.26}$$

One, two, or three values of A may correspond to specified values of δ and $\Sigma_2^{(0)}$. By changing G from zero, the subcritical ax.–r.a. bifurcation point is split into two shape families: one continuous and one with a limit point. The loci of the limit point as G is varied is approximated by the equation

$$\Sigma_2^{(0)} = \tfrac{1}{4}[3B^4\Sigma_{0na}^{(2)}/n^2]^{\frac{1}{3}}, \tag{3.27}$$

which is determined from the condition for a vanishing discriminant and hence is a double root of (3.23). The ruptured bifurcation diagram is shown in figure 3*d*.

(*c*) *Shifting of unbroken bifurcation points*

When the regular perturbations (3.20), (3.21) remain bounded, the variations of the shape families with either G or $\mathscr{V}$ are smooth and the bifurcation points are unbroken. This is so for all of the non-axisymmetric shape families, for the ax.–r.s. points when G is changed, and for the ax.–r.a. points when $\mathscr{V}$ is changed. In accordance with Reiss (1977), the variations of these shape families are estimated by retaining the full two-variable expansion (3.2) but identifying the scaling parameter δ as either G or $\Delta\mathscr{V}$. Several of the lowest-order problems that result have already been solved. For example, the problem of order $\epsilon^0\delta^0$ describes the cylindrical drop shapes; the problems of order $\epsilon^0\delta^1$ are the regular perturbations in G (or $\Delta\mathscr{V}$) that have solutions (3.20),

(3.21); the terms of order $\epsilon^0\delta^1$ describe unperturbed bifurcation from the cylindrical shape family and lead to the four sets of axisymmetric and non-axisymmetric shape families; see § 3.1. The solutions of the problems at order $\epsilon\delta$ describe how the bifurcating families evolve as δ (either G or $\Delta\mathscr{V}$) is varied. The evolution of the sets of bifurcation points is governed by the coefficients $\Sigma_1^{(0)}$ for each point. These coefficients have been calculated for each unbroken bifurcation point and are given in table 2.

4. Computer-aided analysis

The numerical algorithm developed in I for calculating drop shapes, stability, and bifurcation is extended to incorporate more efficient methods for continuing calculations around limit points and for jumping from one family to another at bifurcation points. Also, an algorithm is presented that tracks bifurcation and limit points in two parameters.

The calculations presented here are all of axisymmetric drop shapes and use the finite-element representation of the interface in terms of a set of Hermite cubic polynomials $\{\Phi^i(z)\}$ (Strang & Fix 1973):

$$f(z) = \sum_{i=1}^{N} \chi_i \Phi^i(z) \tag{4.1}$$

where the coefficients $\{\chi_i\}$ are to be determined. In most calculations finite-element bases with either 22 or 44 dimensions were used. This finer discretization was sufficient for all calculations reported here; further increasing the number of elements did not appreciably change the shape of the meniscus or the location of the singular points. Substituting (4.1) into the conditions for an extremum of the potential energy and into the volume constraint yields an $N+1$-dimensional set of algebraic equations,

$$\boldsymbol{R}(\boldsymbol{\alpha}) = \boldsymbol{0}, \tag{4.2}$$

for drop shape and reference pressure $\boldsymbol{\alpha}^{\mathrm{T}} = (\chi_1, \chi_2, \ldots, \chi_N, K)$. Equations (4.2) are solved by Newton's method, which starts from an initial guess $\boldsymbol{\alpha}^{(0)}$ and forms successive iterates $\boldsymbol{\alpha}^{(k)}$ according to

$$\boldsymbol{\alpha}^{(k+1)} = \boldsymbol{\alpha}^{(k)} - \boldsymbol{J}^{-1}\boldsymbol{R}(\boldsymbol{\alpha}^{(k)}). \tag{4.3}$$

The non-zero elements of the Jacobian matrix $\boldsymbol{J}$ are formed analytically as $J_{ij} \equiv \partial R_i/\partial\alpha_j$ and are symmetric ($J_{ij} = J_{ji}$) and banded about the main diagonal. The linear system $\boldsymbol{J}\boldsymbol{\delta}^{(k+1)} = -\boldsymbol{R}(\boldsymbol{\alpha}^{(k)})$, $\boldsymbol{\delta}^{(k+1)} \equiv \boldsymbol{\alpha}^{(k+1)} - \boldsymbol{\alpha}^{(k)}$, is solved by direct factorization of $\boldsymbol{J}$.

Families of drop shapes are calculated by changing sequentially the parameters G, Σ, and $\mathscr{V}$. Continuation methods (Kubicek 1976; Brown *et al.* 1980) are used to calculate a first approximation $\boldsymbol{\alpha}^{(0)}$ for parameter values $(G_0+\Delta G, \Sigma_0+\Delta\Sigma, \mathscr{V}_0+\Delta\mathscr{V})$ slightly different from the set $(G_0, \Sigma_0, \mathscr{V}_0)$, where the solution is known. The initial guess is approximated as

$$\boldsymbol{\alpha}^{(0)}(G_0+\Delta G, \Sigma_0+\Delta\Sigma, \mathscr{V}_0+\Delta\mathscr{V}) = \boldsymbol{\alpha}(G_0, \Sigma_0, \mathscr{V}_0) + \boldsymbol{\alpha}_G\Delta G + \boldsymbol{\alpha}_\Sigma\Delta\Sigma + \boldsymbol{\alpha}_\mathscr{V}\Delta\mathscr{V}. \tag{4.4}$$

The three vectors $(\boldsymbol{\alpha}_G, \boldsymbol{\alpha}_\Sigma, \boldsymbol{\alpha}_\mathscr{V})$ are projections of the $N+4$-dimensional tangents to the surface that describes the family of shapes into the planes corresponding to the parameters $(G, \Sigma, \mathscr{V})$, respectively; for example, $\boldsymbol{\alpha}_\Sigma \equiv (\partial\boldsymbol{\alpha}/\partial\Sigma)_{G,\mathscr{V}}$ evaluated at $\Sigma = \Sigma_0$. Each tangent vector is calculated by solving a linear equation set,

$$\boldsymbol{J}(G_0, \Sigma_0, \mathscr{V}_0)\begin{bmatrix} \boldsymbol{\alpha}_G \\ \boldsymbol{\alpha}_\Sigma \\ \boldsymbol{\alpha}_\mathscr{V} \end{bmatrix} = -\begin{bmatrix} \partial\boldsymbol{R}/\partial G \\ \partial\boldsymbol{R}/\partial\Sigma \\ \partial\boldsymbol{R}/\partial\mathscr{V} \end{bmatrix}_{G_0, \Sigma_0, \mathscr{V}_0}, \tag{4.5}$$

which is of the same form as a Newton iteration.

PHILOSOPHICAL TRANSACTIONS OF THE ROYAL SOCIETY A MATHEMATICAL, PHYSICAL & ENGINEERING SCIENCES

The Jacobian matrix is the finite-dimensional analogue of the linearized operator $\mathscr{L}$ (see equation (3.3)) and becomes singular at bifurcation and limit points. The first singularity is easily detected by monitoring the determinant det (J) along the shape family. This determinant will change sign at a branch point where an eigenvalue of J crosses zero, as in the case for bifurcation with a single null vector. Second- and other even-order multiplicities of the null vectors for J do not change the sign of det (J), but result in the same number of small pivots during the factorization of J. The small pivots can be detected numerically, although not as accurately.

Limit points are more difficult to detect because equilibrium drop shapes, at least in the family being calculated, do not exist beyond the sought parameter value. To circumvent this problem we follow others (Riks 1972; Keller 1977) and define a new parameter s, analogous to arc-length, that increases monotonically along a shape family. The equation set (4.2) is augmented by adding the constraint

$$R_{N+2} = \|\hat{\boldsymbol{\alpha}}\|_\infty - (s - s_0) = 0, \tag{4.6}$$

and the unknowns are supplemented with the parameter λ (either Σ, G, or $\mathscr{V}$) that is being varied. In equation (4.6), $\hat{\boldsymbol{\alpha}}^{\mathrm{T}} \equiv (\alpha_1, \alpha_2, \ldots, \alpha_N, K, \lambda)$ is the new vector of unknowns, s_0 is an arbitrary reference for arc-length set at some point on the shape family and $\|\hat{\boldsymbol{\alpha}}\|_\infty \equiv \max|\hat{\alpha}_i|$, $i = 1, \ldots, N+2$. The augmented equation set (4.2), (4.6) is solved by Newton's method, and the new Jacobian matrix is non-singular at limit points in λ (Keller 1977). Limit points are located by noting when the reciprocals of the components of the tangent vector $(\partial\boldsymbol{\alpha}/\partial\lambda)$ pass through zero.

At a bifurcation point λ^* in a parameter λ (either Σ, G, or $\mathscr{V}$) the Jacobian matrix evaluated at the known drop shape $\boldsymbol{\alpha}(\lambda^*)$ is singular and the equation set (4.5) has a homogeneous solution (null vector) $\boldsymbol{\zeta}$, which is the tangent vector in the direction of the bifurcating shape family. Brown & Scriven (I) constructed first approximations for Newton iterations as $\boldsymbol{\alpha}(\lambda^*) + \epsilon\boldsymbol{\zeta}$ for values of λ near λ^*. The parameter ϵ was varied until the iteration moved away from the shape in the known family and, hopefully, converged to one in the bifurcating family. The procedure is tedious and its success depends strongly on the distance between the two shape families. Several methods have been proposed (Keller 1977; Rheinboldt 1978) that allow more efficient jumping between shape families. We use a method similar to one proposed by Keller (1977) but which gives quadratic convergence to a shape in the new family. It is built around approximating the new shape by

$$\boldsymbol{\alpha}(\lambda) = \boldsymbol{\alpha}(\lambda^*) + \epsilon\boldsymbol{\zeta} + \boldsymbol{\mu}(\lambda), \tag{4.7}$$

where $\boldsymbol{\alpha}(\lambda^*)$ is the known vector at λ^*, $\boldsymbol{\zeta}$ is the null vector, $\boldsymbol{\mu}(\lambda)$ is a correction vector, and ϵ is a non-zero parameter usually taken as ± 0.1. As long as the difference $\lambda - \lambda^*$ is small, the vector $\boldsymbol{\alpha}(\lambda)$ given by (4.7) will have a component orthogonal to the known shape family and cannot belong to this family. To force the solution of equations (4.2) to have the form (4.7), the equation

$$[\boldsymbol{\alpha}(\lambda) - \boldsymbol{\alpha}(\lambda^*)]^{\mathrm{T}}\boldsymbol{\zeta} - \epsilon = 0 \tag{4.8}$$

is added to the set and λ is added to the list of unknowns. The augmented set is solved by Newton's method, starting with the first approximation $\{\boldsymbol{\alpha}(\lambda^*), \lambda^*\}$.

The boundaries of shape stability in terms of the four parameters (Σ, G, $\mathscr{V}$, B) are determined by the loci of singular points in this parameter space. It is prohibitively expensive to calculate singular points by tracking shape families in each of these parameters. Instead we implement an algorithm of Abbott (1978) for locating directly limit and bifurcation points in a parameter λ.

PHILOSOPHICAL TRANSACTIONS OF THE ROYAL SOCIETY A MATHEMATICAL, PHYSICAL & ENGINEERING SCIENCES

To do this, conditions for the occurrence of these singular points are expressed as additional residual equations $\psi(\boldsymbol{\alpha}, \lambda)$. Limit points are given by a vertical tangent $\partial\boldsymbol{\alpha}/\partial\lambda$,

$$\psi(\boldsymbol{\alpha}, \lambda) \equiv \|\partial\boldsymbol{\alpha}/\partial\lambda\|_{\infty}^{-1} = 0, \tag{4.9a}$$

and bifurcation points by the vanishing determinant of the Jacobian matrix,

$$\psi(\boldsymbol{\alpha}, \lambda) \equiv \det(\boldsymbol{J}) = 0. \tag{4.9b}$$

The scheme is to augment the equation set (4.2) with the appropriate condition from (4.9) and to solve simultaneously for $\boldsymbol{\alpha}$ and λ at the singular point. Since there is no efficient way of computing the sensitivity of $\psi(\boldsymbol{\alpha}, \lambda)$ with respect to either $\boldsymbol{\alpha}$ or λ, the augmented equation set is solved by a chord technique that, as shown by Abbott (1978), gives second-order convergence. Starting with an approximation $(\boldsymbol{\alpha}^{(i)}, \lambda^{(i)})$, Newton's method is used to force the drop shape toward one satisfying the conditions for equilibrium:

$$\boldsymbol{\omega}^{(i)} = \boldsymbol{\alpha}^{(i)} - \boldsymbol{J}^{-1}(\boldsymbol{\alpha}^{(i)})\, \boldsymbol{R}(\boldsymbol{\alpha}^{(i)}). \tag{4.10}$$

The tangent vector in the λ-direction along the equilibrium family is then estimated as

$$\boldsymbol{\omega}_{\lambda}^{(i)} \equiv (\partial\boldsymbol{\omega}^{(i)}/\partial\lambda) = -\boldsymbol{J}^{-1}(\boldsymbol{\omega}^{(i)})\, \boldsymbol{R}_{\lambda}(\omega^{(i)}). \tag{4.11}$$

The location of the singular point in λ is estimated as a root of $\psi(\boldsymbol{\alpha}, \lambda)$ by constructing the chord between estimates for two points close to the shape family, $\boldsymbol{\psi}_1 \equiv \psi(\boldsymbol{\omega}^{(i)}, \lambda^{(i)})$ and $\boldsymbol{\psi}_2 \equiv \psi(\boldsymbol{\omega}^{(i)} + \epsilon\boldsymbol{\omega}_{\lambda}^{(i)}, \lambda^{(i)} + \epsilon)$, where the second point is a continuation approximation to the solution at $\lambda^{(i)} + \epsilon$. The best estimate for the vanishing of $\psi(\boldsymbol{\alpha}, \lambda)$ is

$$\lambda^{(i+1)} = \lambda^{(i)} - \epsilon\psi_1/(\psi_2 - \psi_1). \tag{4.12}$$

The solution vector at $\lambda^{(i+1)}$ is approximated by

$$\boldsymbol{\alpha}^{(i+1)} = \boldsymbol{\omega}^{(i)} + (\lambda^{(i+1)} - \lambda^{(i)})\, \boldsymbol{\omega}_{\lambda}^{(i)}, \tag{4.13}$$

and the steps (4.10)–(4.12) are repeated until the change in λ between two iterations is less than a specified value. The accuracy of the algorithm and the convergence criteria depend on the value of ϵ. For most calculations $\epsilon = 10^{-6}$ was used; however, when a limit and bifurcation point were extremely close, a smaller value (10^{-9}) was necessary for convergence of the iteration.

Abbott's method was used to track singular points in λ as a second parameter δ was varied. Once the singular point in λ is known for two values of δ, δ_1 and δ_2, first approximations $(\boldsymbol{\alpha}^{(0)}, \lambda^{(0)})$ for calculating the singular point for $\delta = \delta_3$ are constructed by the finite-difference analogue of the continuation method:

$$\boldsymbol{\alpha}^{(0)}(\delta_3) = \boldsymbol{\alpha}(\delta_2) + \left[\frac{\boldsymbol{\alpha}(\delta_2) - \boldsymbol{\alpha}(\delta_1)}{(\delta_2 - \delta_1)}\right](\delta_3 - \delta_2), \quad \lambda^{(0)}(\delta_3) = \lambda(\delta_2) + \left[\frac{\lambda(\delta_2) - \lambda(\delta_1)}{(\delta_2 - \delta_1)}\right](\delta_3 - \delta_2). \tag{4.14}$$

5. Stability and singular points

Results mentioned in § 1 of the several complete studies of static menisci indicate that the stability of a particular equilibrium shape is related directly to its location in the tree of equilibrium shape families and to the connectivity of each branch, as viewed from bifurcation diagrams such as figure 1. For continuous formulations, like equations (2.1)–(2.4) for a captive drop, this connection has been developed only for specific problems. However, for finite-dimensional problems, such as the finite-element equations (4.2), connections between bifurcation and solution stability

have been rigorously proved. The stability results summarized here all draw from considering the finite-element version of the original continuous problem. We use results generated by two theoretical approaches that differ by the definition of stability used and by the types of equations to which they apply.

The most applicable theories deal with finite-dimensional equation sets that are governed by an energy principle (Thompson & Hunt 1973; Thompson 1979), for this is the case of a static meniscus, and predict how the eigenvalues of the problem for energy stability may change as a parameter is varied through a singular point. The other approach (Iooss & Joseph 1980) is designed for treating finite-dimensional evolution equations: equation sets involving first derivatives with respect to time. Stability to small-amplitude disturbances that have exponential time dependence is analysed and the problem reduces to the calculation of another set of eigenvalues. When an energy principle exists these two approaches give the same stability results, although the energy analysis gives no indication of the decay rates for various disturbances. We take advantage of results from both approaches.

Captive rotating drops may change stability only at singular points. Our discussion is limited to singular points of co-dimension one, i.e. simple bifurcation and limit points, where a single eigenvalue passes through zero; its eigenvector is the shape perturbation that causes instability. These are the only types we found, except for very special values of the parameter sets where two singular points coalesce.

A family of drop shapes must change stability at a limit point in either Σ, G, or $\mathscr{V}$ (Thompson 1977; Iooss & Joseph 1980). If a branch of the family is stable before the limit point, the other branch must be unstable (see figure 1*b*). A limit point in an already unstable family of shapes can either make the drop become unstable or regain stability to an additional disturbance. Examples of all three cases were found by eigenvalue calculations in the shape families of free rotating drops (Brown & Scriven 1980*b*). Thompson (1979) and Katz (1978) have shown that the relative stability of both solution branches near a limit point can be calculated by computing either the energies of shapes along both branches or by calculating a conjugate parameter that measures the rate of change of the energy with respect to introduction of a small amount of the critical eigenfunction at the limit point. Padday & Pitt (1973) used the energy level as the criteria for stability of axisymmetric hydrostatic menisci separating hydrostatic fluids. The stability of the captive drop can be tracked through a succession of limit points by using these criteria.

Stability can be exchanged between two shape families at a simple bifurcation point only in ways dictated by the type of intersection between the families. Under the restriction of a single eigenvalue passing through zero, Iooss & Joseph (1980) show how to reduce this problem to a single dimension projected in the direction of the critical eigenfunction. They prove that each shape family that passes through a simple bifurcation point must change stability unless the family has simultaneously a limit point, as is the case for subcritical (figure 1*a*) or supercritical bifurcation points. Iooss & Joseph also proved that shape families passing through a bifurcation point must have *alternating* stability when evaluated at the same value of the parameter (Σ, $\mathscr{V}$, or G). For example, the two subcritically bifurcating branches on either side of the stable family in figure 1*a* are both unstable, according to these criteria.

The results of Iooss & Joseph are enough to classify completely the stability of branches occurring at the bifurcation point in a shape family that is known *a priori* to be stable for lower values of the parameter. Assessment of the stability of shape families at a bifurcation point is

more difficult when no shapes are known to be stable. As for a limit point, a shape family that is stable on one side of the branch point can *change* stability by becoming more stable or unstable. Deciding which case exists amounts to determining whether the critical eigenfunction at the bifurcation point is the same as the one already causing instability in the shape family. Eigenvalue calculations for shapes on each branch near the bifurcation point are needed to discriminate between these cases. These calculations are not necessary for all values of $\mathscr{V}$ and G, once the stability results are known for the unperturbed ($\mathscr{V} = \pi B$, $G = 0$) case for a range of Σ. The cylindrical, ax.–r.a. and ax.–r.s. shape families each evolve with changes in $\mathscr{V}$ and G. The stability of shapes for the new parameter values is the same as the stability of the unperturbed case, unless the shape family passes through either a limit or bifurcation point.

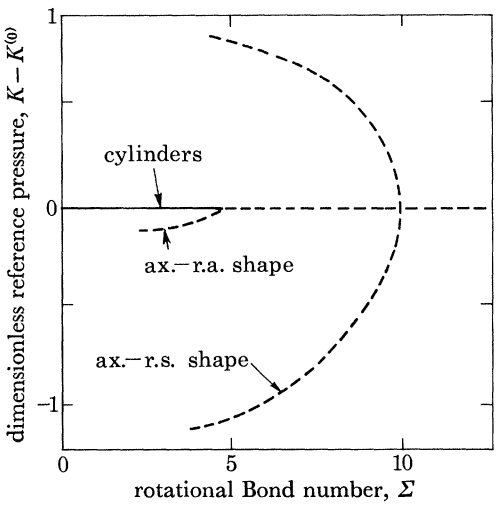

FIGURE 4. Axisymmetric shape families computed by finite-element analysis for $\mathscr{V} = \pi B$, $2B = 1$ and $G = 0$.

6. RESULTS

6.1. *Cylindrical drops*

The unperturbed case of a drop with cylindrical volume $\mathscr{V} = \pi B$ was the starting point for probing variations of drop shape and stability caused by changing any of the four parameters Σ, G, $\mathscr{V}$, and B. From this base, rotating bubbles ($\Sigma < 0$) and drops ($\Sigma > 0$) were studied as a function of drop volume $\mathscr{V}$ and gravitational Bond number. Finite-element calculations were confined to $G > 0$; changing the sign of G amounted to flipping the captive drop and so was redundant. Shape stability was assessed from the guidelines in § 5.

The cylinders and the first two axisymmetric shape families are represented on figure 4 for $2B = 1$. The values of reference pressure $K - K^{(0)}$ were calculated along with drop shapes by the finite-element algorithm. The family of cylindrical shapes lost stability at the branch point to the family of ax.–r.a. shapes, which bifurcated subcritically and were unstable. The ax.–r.s. shape family, predicted to bifurcate transcritically by asymptotics, appears subcritical in figure 4. A much expanded view of the two shape families near the ax.–r.s. bifurcation point (figure 5*b*) shows the acute angle at the crossing, and a nearby limit point in the ax.–r.s. family. As reasoned from the asymptotic analysis, increasing B shifted the limit point through the bifurcation point; the two singular points were numerically coincident at $2B \approx 4.0$. The neighbourhood of the

ax.–r.s. bifurcation point for $2B = 5.5$ is shown in figure 5*a*. The stability of the branches of the ax.–r.s. family could not be determined from the rules in § 5, but eigenvalue calculations in I have shown both branches to be unstable.

Drop shapes belonging to the ax.–r.a. and the two branches of the ax.–r.s. families are shown in figure 6. The menisci became more deformed as the rotational Bond number was decreased along each branch. When gravity was absent, reflecting the ax.–r.a. shapes about the plane $z = 0$ left both as equilibrium shapes, so two distinct branches actually existed, but were superimposed on the projection in the K, Σ-plane. The shapes belonging to the two branches of the ax.–r.s. family were different as shown in figures 6*b*, *c*.

The finite-element calculations made possible a quantitative evaluation of the range of validity of the asymptotic results presented in §3. The slopes and curvatures of the intersections

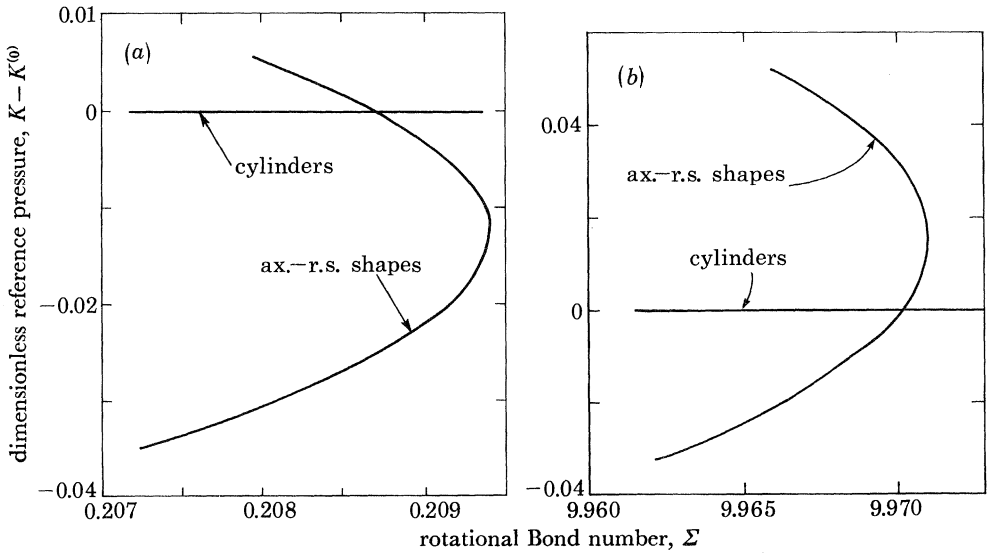

FIGURE 5. Expanded views of the transcritical ax.–r.s. bifurcation point for $G = 0$ and $\forall^{1/3} = \pi B$; (*a*) $2B = 5.5$ and (*b*) $2B = 1$.

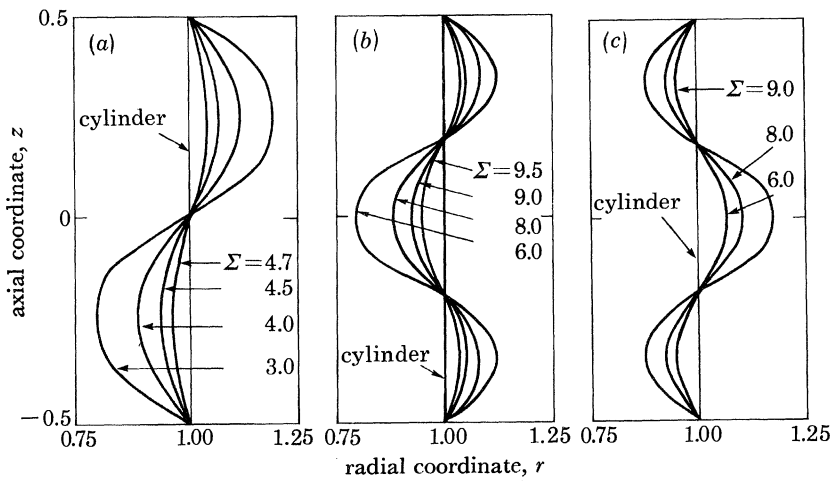

FIGURE 6. Drop shapes for $\forall^{1/3} = \pi B$, $G = 0$ and $2B = 1$. Shapes are from (*a*) the ax.–r.a. family, (*b*) the upper branch of the ax.–r.s. family and (*c*) the lower branch of the ax.–r.s. family.

of the r.a. and r.s. bifurcating families with the cylindrical families are given in table 3 for both asymptotic and numerical calculations. Over a small range of Σ both agreed well. As expected, the range of validity of the results about the ax.–r.s. family was constricted by the nearby limit point.

6.2. *Changes in drop volume*

Decreasing the volume of the drop caused the cylindrical shapes to draw inward at their waists. These new shapes are reflectively symmetric about $z = 0$ and so have the same symmetry as the shapes in the ax.–r.s. family. The projection of the axisymmetric shape families into the K, Σ-plane is shown in figure 7 for $\mathscr{V} = 0.75\pi B$ and $2B = 1.0$. For small changes in $\mathscr{V}$, the bifurcation point between what were the cylindrical and ax.–r.s. shape families was ruptured and a limit point was created. The bifurcation between the ax.–r.a. and cylindrical shape families

TABLE 3. COMPARISON OF COEFFICIENTS PREDICTED BY ASYMPTOTIC ANALYSIS AND FINITE-ELEMENT CALCULATIONS

bifurcation point		quantity	asymptotic result	numerical results	range of validity in terms of parameter
ax.–r.a.	unperturbed	$\Sigma_0^{(2)}/K_0^{(2)}$	17.0	15.7	$\Delta\Sigma < 1$
ax.–r.s.	unperturbed	$\Sigma_0^{(1)}/K_0^{(1)}$	-0.126	-0.125	$\Delta\Sigma < 10^{-4}$
ax.–r.a.	perturbed in $\mathscr{V}$	$\Sigma_1^{(1)}$	-1.45	-1.45	$\Delta\mathscr{V} < 10^{-2}$
ax.–r.a.	perturbed in G	$\Sigma_2^{(0)}$	-0.57	-0.55	$\Delta G < 1$
ax.–r.s.	perturbed in $\mathscr{V}$	$\Sigma_1^{(0)}$	-1.79 $(2B = 1.0)$ -0.030 $(2B = 5.5)$	< -2.5 -0.024	$\Delta\mathscr{V} < 10^{-5}$ $\Delta\mathscr{V} < 10^{-4}$
ax.–r.s.	perturbed in G	$\Sigma_1^{(0)}$	0	—	—
n.ax.–r.s.	perturbed in $\mathscr{V}$	$\Sigma_1^{(0)}$	-0.89	-0.95	$\Delta\mathscr{V} < 10^{-2}$
n.ax.–r.a.	perturbed in G	$\Sigma_1^{(0)}$	0	—	—

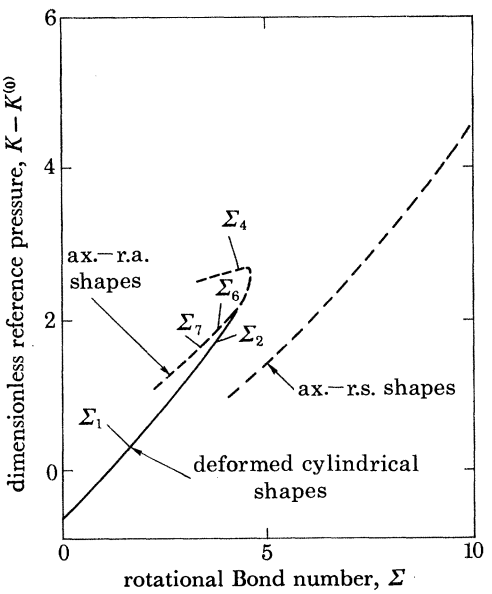

FIGURE 7. Axisymmetric shape families computed for $\mathscr{V} = 0.75\pi B$, $2B = 1$, and $G = 0$. The rupturing of the main shape family at the ax.–r.s. bifurcation point, and the disconnected shape families are shown. Unstable drop shapes are given as dashed lines (- - -). The Σ-values (Σ_i) correspond to drop shapes shown in figure 8.

still occurred at a value of Σ lower than for the new limit point. Meniscus shapes along the two distinct families for $\mathscr{V} = 0.75\pi B$ are given in figure 8; the symmetries of the shapes in the unperturbed families ($\mathscr{V} = \pi B$) remained, but were superimposed on the deformed drop shapes.

Decreasing the drop volume further moved the limit point to a lower value of Σ and moved it closer to the ax.–r.a. bifurcation point. On the bifurcation diagram for $\mathscr{V} = 0.5\pi B$ and $2B = 1.0$ (figure 9), the order of the bifurcation and limit points was reversed and the drop first lost stability (and local equilibrium) at the limit point. The loci of the ax.–r.a. bifurcation points and the limit points have been calculated by the scheme explained in § 4 and are shown in figures 10 and 11 for $2B = 1.0$ and $2B = 5.5$, respectively. In both cases, the limit point created from the

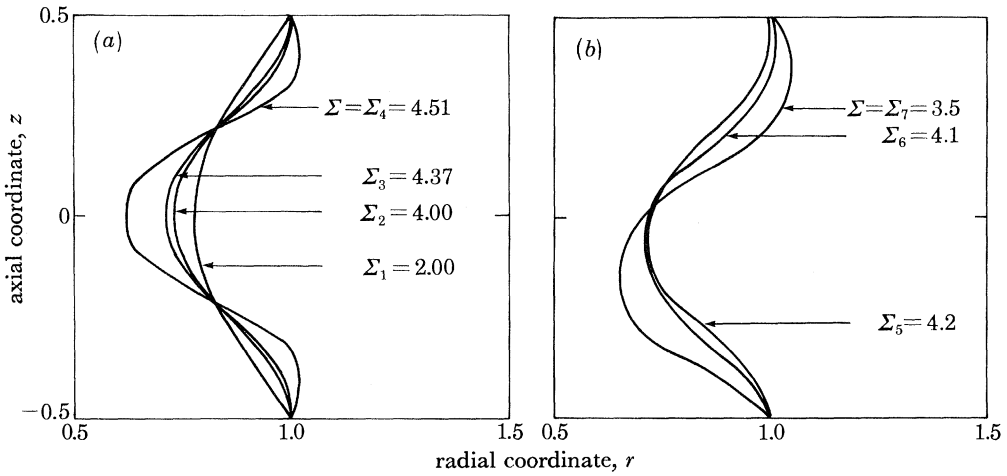

FIGURE 8. Sample drop shapes for $\mathscr{V} = 0.75\pi B$, $2B = 1$, and $G = 0$: (*a*) shapes in families of deformed cylinders; (*b*) shapes in ax.–r.a. family.

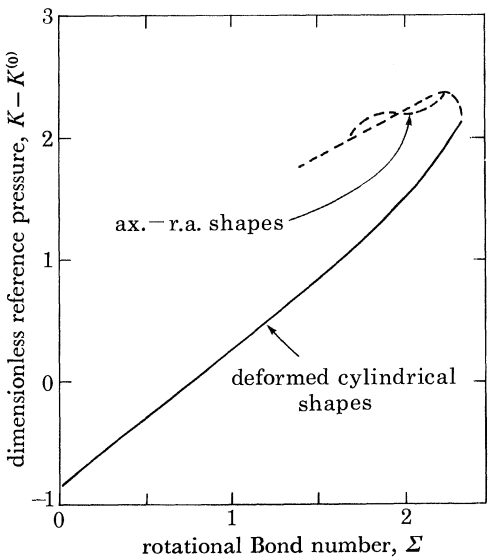

FIGURE 9. Axisymmetric shape families computed for $\mathscr{V} = 0.5\pi B$, $2B = 1$, and $G = 0$. Unstable drop shapes are given as dashed curves (- - -).

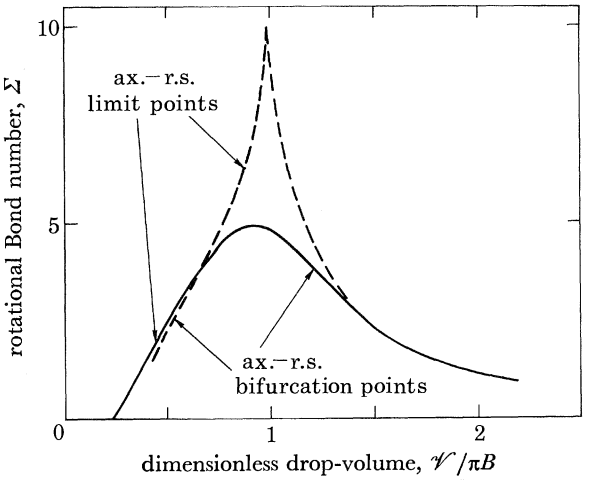

FIGURE 10. Variation of the values of rotational Bond number for ax.–r.a. bifurcation and ax.–r.s. limit points with drop volume for $2B = 1.0$ and $G = 0$. Solid curves indicate the mode responsible for loss of stability of the drop.

ax.–r.s. families decreased rapidly as $\mathscr{V}$ changed from πB compared with changes in the value of Σ for the ax.–r.a. bifurcation point. This behaviour is expected because of the quadratic dependence of $\mathscr{V}$ on Σ near that limit point which was predicted by the asymptotic results.

The loci of the bifurcation and limit points were coincident for a drop of dimensionless volume $\mathscr{V} = 0.6\pi B$. This result was not accurately predicted by the analysis of § 3. The curve of ax.–r.a. bifurcation points had a maximum in Σ for a drop with slightly less volume than a cylinder. This made the asymptotic behaviour of the curve near $\mathscr{V} = \pi B$ unrepresentative of that at small values of $\mathscr{V}$. Projected in the $\mathscr{V}$, Σ-plane of figure 10, the intersection point of the two families of singular points appeared numerically as a cusp point (Iooss & Joseph 1980); the two curves intersected but did not cross. For dimensionless volumes less than $\mathscr{V} = 0.6\pi B$, the limit point appeared first in the stable shape family. The mode of instability had shifted from an ax.–r.a. shape instability associated with the subcritical bifurcation to a reflectively symmetric perturbation caused by the limit point; see figures 7 and 9.

TABLE 4. COORDINATES $(B, \mathscr{V}, G)$ FOR THE COINCIDENCE OF THE AX.–R.A. BIFURCATION POINT AND THE AX.–R.S. LIMIT POINT

drop length, $2B$	dimensionless volume, $\mathscr{V}/\pi B$	rotational Bond number, Σ
1.0	0.60	3.20
1.4	0.54	1.75
2.0	0.53	0.88
3.0	0.55	0.26
4.0	0.58	0.03
5.5	0.60	−0.15

Increasing the drop volume decreased the rotational Bond numbers for the bifurcation and limit points and brought them close together. They were not coincident up to the largest drop volume that could be accommodated in the cylindrical representation used here. Increasing the length of the drop to $2B = 5.5$ (figure 11) did not change the structure of the bifurcation and limit point curves, but shifted them to lower values of Σ. The cusp point between the curves occurred at $\Sigma = -0.15$ corresponding to a rotating bubble. Again, the asymptotic analysis gave a poor prediction of the cusp point; this was clearly seen by drawing tangents to both curves on figure 11 at $\mathscr{V} = \pi B$.

The variation of the point for the exchange of instability mode with drop length is shown in table 4. The rotational Bond number Σ decreased monotonically with increasing B. The drop volume for the switch in the mode of instability passed through a shallow minimum near $B = 1.0$.

Gillette & Dyson (1971) have shown that non-rotating captive drops which are neutrally buoyant ($G = 0$) and of fixed volume may be unstable. They established upper and lower bounds on the drop volume for a range of values of drop length. We have used the algorithm for tracking singular points to trace out the neutral stability curve in the B, $\mathscr{V}$-plane that corresponds to the low bound of Gillette & Dyson; this result is shown in figure 12. The upper bounds on drop volume all correspond to drop shapes that bulge from the discs and cannot be represented as $f = f(z, \theta)$. The well known Rayleigh (1879) limit is the neutrally stable cylindrical ($\mathscr{V} = \pi B$) drop with $2B = 2\pi$. Non-rotating drops with $2B < 4.1$ lost stability to an ax.–r.a. perturbation, whereas drops of greater length lost equilibrium at the limit point caused by the rupturing of the first ax.–r.s. shape family. This crossing point is seen by examining table 4.

The asymptotic and numerical predictions for the slopes $d\Sigma/d\mathscr{V}$ at the cylindrical family are given in table 3 for the intersections of the first ax.–r.a., ax.–r.s., and non-axisymmetric shape families. The numerical results for the non-axisymmetric shape family were taken from data presented in I. The bifurcation points to the non-axisymmetric and ax.–r.a. families are not ruptured by changes in $\mathscr{V}$, and the asymptotic results had comparable ranges of validity in both cases. The limit point in the ax.–r.s. family again caused the asymptotic results to be inaccurate. Even for changes in volume of 10^{-5}, asymptotic and finite-element results agreed only to within 50 % for $2B = 1.0$. This accuracy was improved slightly at $2B = 5.5$, where the limit point is farther from the bifurcation point in the unperturbed (cylindrical) case; see figure 5.

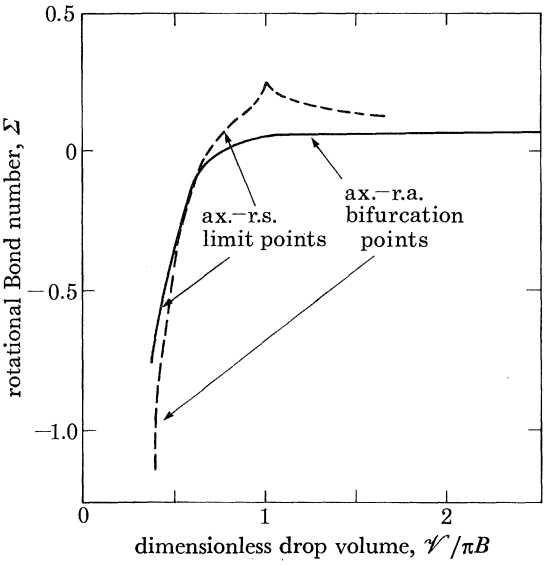

FIGURE 11. Variation of the values of rotational Bond number with drop volume for ax.–r.a. bifurcation and ax.–r.s. limit points, for $2B = 5.5$ and $G = 0$. Solid curves indicate the mode responsible for loss of stability of the drop.

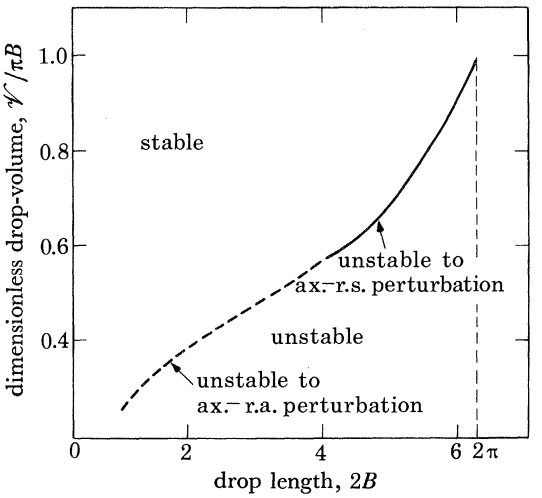

FIGURE 12. Neutral stability curve for non-rotating ($\Sigma = 0$), neutrally buoyant captive drops ($G = 0$). Dashed (- - -) curve indicates change in the mode of instability.

6.3. *Changes in gravitational Bond number*

Increasing G from zero caused shapes in the cylindrical family to sag toward the plane $z = 0$. Drop shapes for $\Sigma = 0$, $G = 10$, $B = 1$, and a range of drop volumes are shown in figure 13. Note that shapes for drops with volume very much greater than the cylinder (e.g. $\mathscr{V} = 2\pi B$) cannot be represented adequately in cylindrical coordinates. These shapes appear to be resting on an imaginary surface when they should sag below the plane perpendicular to the axis at $z = -B$. We limited our calculations to drops with almost cylindrical volume or to long drops ($2B > 1$) where the representation was valid for a wider range of $\mathscr{V}$. For non-zero G, the ax.–r.a. shape family was ruptured and a limit point was formed where the drop lost stability. The limit point moved rapidly to smaller values of Σ with increasing G. As shown in table 3, the asymptotic results accurately predicted the rate of decrease of Σ with G for gravitational Bond numbers up to unity. The ax.–r.s. bifurcation point was not broken by changes in G, as predicted by asymptotics. To first order, this bifurcation point was stationary for changes in G. No attempt was made at numerically estimating the curvature of this family in the Σ, G-plane.

The limit of stability of a drop of length $2B = 5.5$ is given in figure 14 for $\mathscr{V} = \pi B$. Again all drops lost stability to an ax.–r.a. perturbation at the limit point. For $G \equiv 0.028$, the static drop ($\Sigma = 0$) lost stability. The loci of this hydrostatic instability is shown on figure 15 as a function of drop length. The points shown on this figure were taken from Coriell *et al.* (1977) and agree well with our calculations. The effect of drop volume on the hydrostatic limit is demonstrated on figure 16 for $2B = 5.5$. As the volume was decreased, the critical value of G also decreased until, at $\mathscr{V} \approx 0.79\pi B$, the drop volume became unstable without gravity. This point corresponded to the lower limit of Gillette & Dyson; see figure 12. At large drop volumes the locus of instability in the $\mathscr{V}$, G-plane must have a maximum and pass through Gillette & Dyson's upper bound on

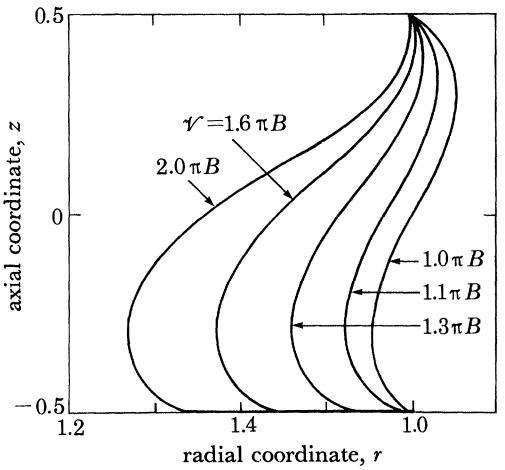

FIGURE 13. Sample shapes of non-rotating ($\Sigma = 0$) drops with $G = 10$, $2B = 1$, and drop volumes between πB and $2\pi B$.

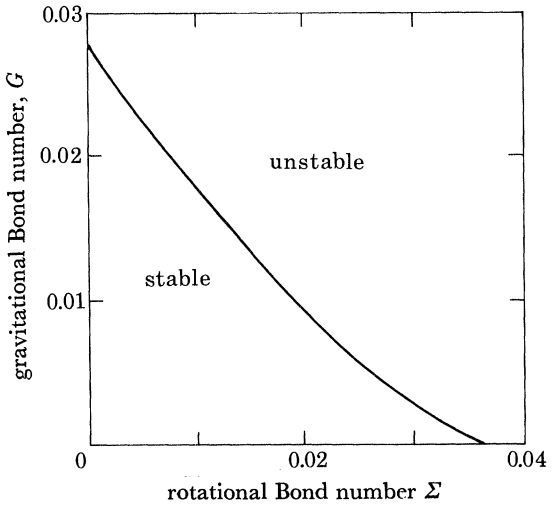

FIGURE 14. Effect of gravitational Bond number of ax.–r.a. limit point for $\mathscr{V} = \pi B$ and $2B = 5.5$. This is also the neutral stability curve.

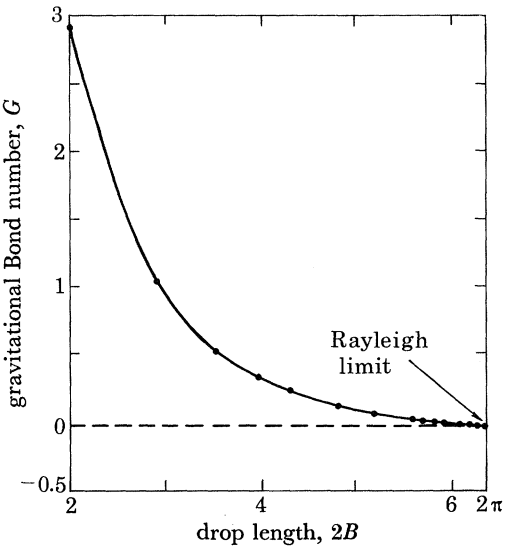

FIGURE 15. Neutral stability curve for non-rotating ($\Sigma = 0$) drops with $\mathscr{V} = \pi B$. Points are from Coriell *et al.* (1977).

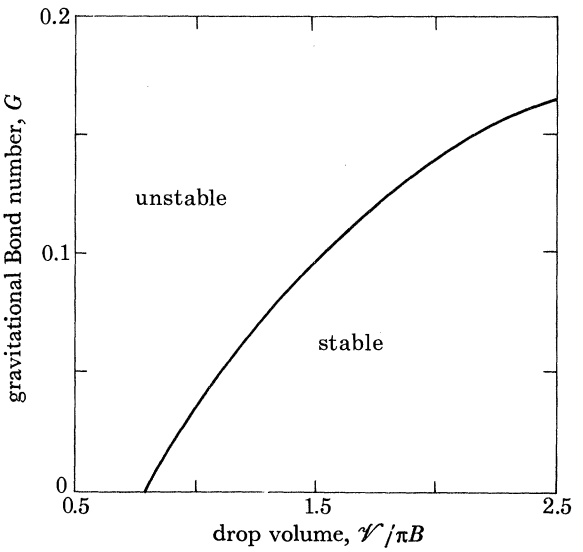

FIGURE 16. Effect of drop volume on gravitational Bond number for ax.–r.a. limit point with $\Sigma = 0$ and $2B = 5.5$. This is also the neutral stability curve.

drop volume for stability at $G = 0$. Unfortunately, the cylindrical shape representation failed long before either point was reached. Boucher & Evans (1980) also studied the stability of captive drops in the $\mathscr{V}$, G-plane and our results agree as closely as can be estimated from their plots.

7. Concluding remarks

A complete picture of the shape and stability of captive rotating drops must include the non-axisymmetric equilibria which are neglected in § 6. Non-axisymmetric shapes bifurcate first from the cylindrical family as long as the drop length satisfies the criteria $2B < \pi\sqrt{3}$; this is the case for our calculations with $2B = 1$. Finite-element calculations reported in I have shown that the $n = 1$ non-axisymmetric bifurcation point still governs drop instability when the drop volume is perturbed from the cylinder. The exact range of $\mathscr{V}$ depended on the drop length; for drops significantly larger or smaller than a cylinder, the rotational Bond number for bifurcation to the n.ax.–r.s. family decreased from its value for $\mathscr{V} = \pi B$. For even larger and smaller drops the mode for instability must change from the non-axisymmetric one to an axisymmetric shape because axisymmetric perturbations are most dangerous to the stability of hydrostatic ($\Sigma = 0$) menisci that are axisymmetric (Coriell *et al.* 1977). Comparing figure 10 in I with figure 10 here shows that the mode has not changed for drop volumes between $0.5\pi B \leqslant \mathscr{V} \leqslant 1.6\pi B$ when $2B = 1$; however, this change is shown for $2B = 2$ in figure 11 in I.

Drops with length $2B = 5.5 (> \pi\sqrt{3})$ are first unstable to an axisymmetric mode and so results presented here give the entire picture of equilibrium shape and stability. Stable and unstable equilibrium forms are separated by a surface drawn in the coordinate space $(\Sigma, \mathscr{V}, G)$ that has projections onto the coordinate axis given by figures 11, 14 and 16. The surface is convex around the non-rotating cylindrical shape $(0, \pi B, 0)$, and all drops on this side of the surface are stable. The shape perturbations that populate the surface and cause instability are associated with either limit or bifurcation points, depending on the values of Σ, $\mathscr{V}$, and G. Understanding the evolution, in terms of parameters of both stable and unstable shape families, is necessary to explain the behaviour of any nonlinear iterative scheme for calculating equilibrium shapes. Coriell *et al.* (1977) used a shooting technique to calculate axisymmetric shapes of rotating captive drops with gravity. They reported that in some cases the iterations converged to static shapes that either bulged at the top (with respect to gravity) or satisfied $\mathrm{d}f/\mathrm{d}z = 0$ at more than two values of z, instead of the more expected shapes like those in figure 13. The multiple-equilibrium shapes of Coriell *et al.* are members of the different ax.–r.a. and ax.–r.s. shape families described here. Their shooting algorithm jumped between equilibria in different shape families because of changes in the initial guess supplied to the algorithm. Methods are available (Keller 1969) for studying bifurcation points in two-point boundary value problems that are solved by initial-value methods like those of Coriell *et al.* and have been applied to simple two-dimensional meniscus problems (Brown 1979).

Neither changes in drop volume nor changes in gravitational Bond number cause imperfections in the bifurcation points between the cylindrical and the non-axisymmetric shape families. In principle, all bifurcation points are structurally unstable (Thompson & Hunt 1975) and are ruptured by some change in the parameters of the system. The solvability criteria (3.7) show the development of an imperfection to be related directly to the symmetry relation between the changes in drop shape caused by varying a particular parameter and the eigenfunction that describes the unperturbed bifurcating shapes. More exactly, these two functions must have the

same symmetry for an imperfection to develop. This is the case for changes in drop volume and the ax.–r.s. shapes, as well as for changes in G and the ax.–r.a. shapes. The bifurcations to the non-axisymmetric shape families are only broken by introducing azimuthal asymmetries into the ideal system. The most likely source is the misalignment of the two discs, which would cause the drop to bulge in one direction and break the first non-axisymmetric bifurcation point. The bifurcation points to non-axisymmetric shapes can also be broken intentionally by shaping the discs in the form of the preferred multi-lobed drop, i.e. $f(-B,\theta) = f(B,\theta) = 1 + d\cos(n\theta)$, where d is a constant. Whether or not the new limit point will represent the limit of shape stability will depend on the parameters $(\mathscr{V}, G, \Sigma)$ and on the deformation of the discs as measured by d.

Imperfections that break symmetry and rupture bifurcation points can be identified in other capillary problems. For example, the mechanism for rupturing a charged spherical drop (Rayleigh 1882) changes from a subcritical bifurcation to a family of two-lobed drop shapes to a limit point in a family of the same symmetry (Taylor 1966) when an external electric field is introduced. Michael *et al.* (1974, 1975) also observed the breaking of a bifurcation point into a limit point in the families of shapes of a layer of insulating liquid separating conducting fluids at different electrostatic potentials. Also, the bifurcation points to non-axisymmetric shape families where axisymmetric sessile and certain pendent drops lose stability (see Michael 1981) are both ruptured by inclining the drop so that it is no longer axisymmetric (Lawal & Brown 1982*a*, *b*).

Imperfections that rupture bifurcations are particularly important because the singular nature of the imperfection implies a very rapid change in the critical point for small changes in the imperfection parameter. This gives the typical cusp shape on plots of the critical point against the parameter seen in figures 10 and 11. Asymptotic analysis, like that presented in § 3.2 usefully characterizes the sensitivity of bifurcation points to imperfections caused by introducing other parameters, however, it does not always give accurate estimates of the variation of the critical point over ranges of the parameter large enough to infer the interaction of that critical point with others. The limited ranges of validity of the asymptotic results are clearly seen in the results of §§ 6.2 and 6.3. Numerical calculation by techniques specifically for tracking limit and bifurcation points must be used to study a wide range of parameters.

This research was partially supported by the Eastman Kodak Company, by the Materials Processing Program of the U.S. National Aeronautics and Space Administration, and by the National Science Foundation through a fellowship to L.H.U. The authors are grateful to O. A. Basaran and R. E. Benner for independently calculating equations (3.3), (3.4) and to A. Lawal for valuable discussions on numerical methods.

References

Abbott, J. P. 1978 An efficient algorithm for the determination of certain bifurcation points. *J. Comput. appl. Math.* **4**, 19–26.

Benner, Jr, R. E., Basaran, O. A. & Scriven, L. E. 1980 Stability and bifurcation of translationally symmetric, rotating liquid drops. *Bull. Am. phys. Soc.* **25**, 1073.

Boucher, E. A. & Evans, M. J. B. 1980 Capillary phenomena. XII. Properties of fluid bridges between solids in a gravitational field. *J. Colloid Interface Sci.* **75**, 409–418.

Brown, R. A. 1979 The shape and stability of three-dimensional interfaces. Ph.D. thesis, University of Minnesota.

Brown, R. A. & Scriven, L. E. 1980*a* The shapes and stability of captive rotating drops. *Phil. Trans. R. Soc. Lond.* A **297**, 51–79. (Paper I.)

Brown, R. A. & Scriven, L. E. 1980*b* The shape and stability of rotating liquid drops. *Proc. R. Soc. Lond.* A **371**, 331–357.

Brown, R. A. & Scriven, L. E. 1980*c* On the multiple equilibrium shapes and stability of an interface pinned on a slot. *J. Colloid Interface Sci.* **78**, 528–542.

Brown, R. A., Scriven, L. E. & Silliman, W. J. 1980 Computer-aided analysis of nonlinear problems in transport phenomena. In *New approaches to nonlinear problems in dynamics* (ed. P. J. Holmes). Philadelphia: Society for Industrial and Applied Mathematics.

Coriell, S. R., Hardy, S. C. & Cordes, M. R. 1977 Stability of liquid zones. *J. Colloid Interface Sci.* **60**, 126–136.

Friedman, B. 1956 *Principles and techniques of applied mathematics*. New York: Wiley.

Gillette, W. A. & Dyson, D. C. 1971 Stability of fluid interfaces of revolution between equal solid circular plates. *Chem. Engng J.* **2**, 44–54.

Iooss, G. & Joseph, D. D. 1980 *Elementary stability and bifurcation theory*. New York: Springer-Verlag.

Katz, J. 1978 On the number of unstable modes of an equilibrium. *Mon. Not. R. astr. Soc.* **183**, 765–769.

Keener, J. P. & Keller, H. B. 1973 Perturbed bifurcation theory. *Arch. ration. Mech. Analysis* **50**, 159–175.

Keller, J. B. 1969 Bifurcation theory for ordinary differential equations. In *Bifurcation theory and nonlinear eigenvalue problems* (ed. J. B. Keller & S. Autman). New York: Benjamin.

Keller, H. B. 1977 Numerical solution of bifurcation and nonlinear eigenvalue problems. In *Applications of bifurcation theory* (ed. P. H. Rabinowitz). New York: Academic Press.

Kubicek, M. 1976 Dependence of solution of nonlinear equations on a parameter. *ACM Trans. math. Software* **2**, 98–107.

Lawal, A. & Brown, R. A. 1982*a* The stability of an inclined pendent drop. *J. Colloid Interface Sci.* (In the press.)

Lawal, A. & Brown, R. A. 1982*b* The stability of an inclined sessile drop. *J. Colloid Interface Sci.* (Submitted.)

Majumdar, S. R. & Michael, D. H. 1976 The equilibrium and stability of two-dimensional pendent drops. *Proc. R. Soc. Lond.* A **351**, 89–115.

Matkowsky, B. J. & Reiss, E. L. 1977 Singular perturbations of bifurcations. *SIAM Jl appl. Math.* **33**, 230–255.

Michael, D. H. 1981 Meniscus stability. *A. Rev. Fluid Mech.* **13**, 189–215.

Michael, D. H., Norbury, J. & O'Neil, M. E. 1974 Electrohydrostatic instability in electrically stressed dielectric fluids. Part 1. *J. Fluid Mech.* **66**, 289–308.

Michael, D. H., Norbury, J. & O'Neil, M. E. 1975 Electrohydrostatic instability in electrically stressed dielectric fluids. Part 2. *J. Fluid Mech.* **72**, 95–112.

Padday, J. F. & Pitt, A. R. 1973 The stability of axisymmetric menisci. *Phil. Trans. R. Soc. Lond.* A **275**, 489–528.

Pimbley, Jr, G. H. 1976 Stationary solutions of the problem of Rayleigh–Taylor instability. *J. math. Anal. Appl.* **55**, 170–206.

Pitts, E. 1973 The stability of pendent liquid drops. Part I. Drops formed in a narrow gap. *J. Fluid Mech.* **59**, 753–767.

Pitts, E. 1976 The stability of a drop hanging from a tube. *J. Inst. Math. Applics* **17**, 387–397.

Rayleigh, Lord 1879 On the instability of jets. *Proc. Lond. math. Soc.* **10**, 4–13.

Rayleigh, Lord 1882 On the equilibrium of liquid conducting masses charged with electricity. *Phil. Mag.* **14**, 184–186.

Reiss, E. L. 1977 Imperfect bifurcation. In *Applications of bifurcation theory* (ed. P. H. Rabinowitz). New York: Academic Press.

Rheinboldt, W. C. 1978 Numerical methods for a class of finite dimensional bifurcation problems. *SIAM Jl numer. Anal.* **15**, 1–11.

Riks, E. 1972 The application of Newton's method to the problem of elastic stability. *J. appl. Mech.* **39**, 1060–1065.

Strang, G. & Fix, G. J. 1973 *An analysis of the finite element method*. Englewood Cliffs, New Jersey: Prentice Hall.

Taylor, Sir Geoffrey 1966 Disintegration of water drops in an elastic field. *Proc. R. Soc. Lond.* A **291**, 383–397.

Thompson, J. M. T. 1979 Stability predictions through a succession of folds. *Phil. Trans. R. Soc. Lond.* A **292**, 1–23.

Thompson, J. M. T. & Hunt, G. W. 1973 *A general theory of elastic stability*. London: Wiley.

Thompson, J. M. T. & Hunt, G. W. 1975 Towards a unified bifurcation theory. *Z. angew. Math. Phys.* **26**, 581–604.

PHILOSOPHICAL TRANSACTIONS OF THE ROYAL SOCIETY A MATHEMATICAL, PHYSICAL & ENGINEERING SCIENCES